C. R. Physique 17 (2016) 471–480

Contents lists available at ScienceDirect

Comptes Rendus Physique

www.sciencedirect.com

Condensed matter physics in the 21st century: The legacy of Jacques Friedel

Insulating oxide surfaces and nanostructures

Surfaces d'oxyde isolantes et nanostructures

Jacek Goniakowski [a,b], Claudine Noguera [a,b,*]

[a] *CNRS, Institut des Nanosciences de Paris, UMR 7588, 4, place Jussieu, 75005 Paris, France*
[b] *UPMC Université Paris-6, INSP, UMR 7588, 4, place Jussieu, 75252 Paris cedex 05, France*

ARTICLE INFO

Article history:
Available online 14 December 2015

Keywords:
Oxides
Surfaces
Nanostructures
Gap
Tight-binding methods
Ultra-thin films

Mots-clés :
Oxydes
Surfaces
Nanostructures
Gap
Méthodes *tight-binding*
Films ultra-fins

ABSTRACT

This contribution describes some peculiarities of the science of oxide surfaces and nanostructures and proposes a simple conceptual scheme to understand their electronic structure, in the spirit of Jacques Friedel's work. Major results on the effects of non-stoichiometry and polarity are presented, for both semi-infinite surfaces and ultra-thin films, and promising lines of research for the near future are sketched.

RÉSUMÉ

Cet article décrit quelques particularités de la science des surfaces d'oxydes et des nanostructures, et propose un schéma conceptuel simple permettant de comprendre leur structure électronique, dans l'esprit des travaux de Jacques Friedel. Des résultats majeurs quant aux effets de non-stœchiométrie et de polarité sont presentés, à la fois pour les surfaces semi-infinies et les films ultra-fins, et des perspectives de recherche prometteuses pour un future proche sont esquissées.

1. Introduction

Understanding the characteristics of surfaces, which are the contact zones between a solid and its environment, is of crucial interest from many points of view. However, while metal surfaces have been studied for more than fifty years with techniques of increasing sophistication, the science of oxide surfaces has only emerged in the late 1990s [1]. This delay was due more to experimental difficulties and theoretical disinterest than to the materials themselves. As a matter of fact, it took a long time to realize that very specific protocols of sample preparation were needed to control the surface stoichiometry and thus to achieve surface reproducibility. Moreover, the insulating character of numerous oxides induces charging effects when electrons are sent to or collected from their surfaces during spectroscopic experiments, making it difficult to correctly calibrate the sought information. The use of scanning tunneling microscopy (STM) is also impossible,

* Corresponding author at: CNRS, Institut des Nanosciences de Paris, UMR 7588, 4, place Jussieu, 75005 Paris, France.
E-mail address: Claudine.Noguera@insp.jussieu.fr (C. Noguera).

http://dx.doi.org/10.1016/j.crhy.2015.12.007
1631-0705/

unless oxides are sufficiently doped or deposited as thin films on a metal substrate. From the point of view of theory, a description of insulating oxides in terms of classical charges has long been considered as sufficient, driving the interest of theorists to more fashionable materials. Eventually, experimental and theoretical advances have been made, highlighting novel structural and electronic effects not met in more traditional materials. This has revived activity in various disciplinary fields, such as mineralogy, geochemistry, toxicology, catalysis, electronics, spintronics, and has even led to the emergence of the recent "all-oxide" electronics.

For a long time, all insulating oxides have been described by classical electrostatic models, in which the ionic charges play the major role. This has led to the development of the Born model of cohesion in which the leading interatomic forces result from Coulomb charge–charge interactions, to which short-range repulsion and weak van der Waals terms are added [2]:

$$E = \frac{1}{2}\sum_{i\neq j}\left(\frac{Q_i Q_j}{r_{ij}} + B_{ij}\,\mathrm{e}^{-\frac{r_{ij}}{\rho}} - \frac{C_{ij}}{r_{ij}^6}\right) \tag{1}$$

Such models have been widely used in the past, for example to predict inorganic crystal structures, relaxation effects at oxide surfaces but also lattice dynamics or point defect properties [3,4]. Even now, they remain useful to understand complex mineral bulk or surface structures [5] or to derive structural phase diagrams of mixed oxides [6]. However, because they include no information on the electronic structure, their parameters determined for bulk atom environment are not necessarily transferable to surfaces or nano-objects.

The development of concepts such as local electronegativity or site specific acid/base character [1], has lead to the recognition that, even in highly ionic materials, the electronic structure is not frozen but may vary as a function of the local environment of the atoms. Methods intermediate between fully classical and fully quantum methods have emerged, such as those based on the electronegativity equalization principle [7–9] which yield environment dependent ionic charges. They are very efficient to address issues in which large systems are involved. This was, for example, the case in the impressive molecular dynamic simulation of the oxidation of an aluminum nanoparticle, in which interactions between more than eight hundred thousand atoms were accounted for [10]. However, these methods still disregard many essential electronic characteristics.

In particular, they are unable to give an interpretation of the forbidden gap in insulating oxides. The latter may be associated either with a transfer of electron from an oxygen ion to a cation ($X^{n+} + O^{--} \rightarrow X^{(n-1)+} + O^{-}$) or with an exchange of electrons between two cations ($X^{n+} + X^{n+} \rightarrow X^{(n-1)+} + X^{(n+1)+}$). In the first case, the excitation energy Δ_{CT} is equal to the difference between the oxygen second electronic affinity A_2 and the cation nth ionization potential I_n, while in the second case, the excitation energy Δ_U is related to the difference between the $(n+1)$th and nth cation ionization potentials I_{n+1} and I_n. According to whether $\Delta_{CT} < \Delta_U$ or $\Delta_{CT} > \Delta_U$, the insulators are of charge-transfer or of Mott–Hubbard type [11]. Simple oxides such as MgO, Al_2O_3, SiO_2 and d^0 transition metal oxides, such as TiO_2 or $SrTiO_3$ are charge-transfer insulators, while most other transition metal oxides are Mott–Hubbard ones. These latter usually require more advanced simulation methods to account for their electronic structure than the former.

In the last decades, the description of the electronic structure of materials has impressively improved, at a level of quasi-chemical accuracy [12,13]. Density Functional Theory (DFT), in its various implementations, is a widely used tool which, in most cases, satisfactorily predicts atomic structures but may fail in correctly accounting for some electronic properties. The reasons why it largely under-estimates the gap width of insulators and is unable to yield good quasi particle spectra have been assigned to the lack of correct treatment of exchange [14] which yields erroneous self-interaction energy terms [15]. In the following section, in the spirit of Jacques Friedel's work, we will present a simplified description of the electronic structure of insulating oxides, which only retains the key ingredients and may thus be used to interpret the mechanisms taking place at their surfaces or around low-coordinated atoms in nano-objects.

2. Simple approach to the electronic structure of insulating oxides

In transition metals and tetrahedral semi-conductors, the tight-binding method — which is the equivalent of the Linear Combination of Atomic Orbitals (LCAO) in chemistry — has been very successful to predict band structures, density of states (DOS) and Fermi level position, before the advent of ab initio methods. It is based on the resolution of an effective one-electron Schrödinger equation, projected on a minimal basis set made of atomic orbitals which are assumed orthogonal. In its simplest form, only two types of Hamiltonian matrix elements are kept: the diagonal ones which represent the (effective) atomic orbital energies ϵ_i, and the non-diagonal ones β_{ij}, named resonance or hopping integrals, which involve orbitals on neighboring atoms. The latter are responsible for the formation of bands and electron delocalization. Generic features of the local DOS (LDOS) may then be obtained, such as its center of gravity related to the ϵ_i and its width $W \propto \beta\sqrt{Z}$, which was shown to scale as the square root of the local atomic coordination number Z [16].

Application of this method allowed for example J. Friedel to analyze the dependence of the bulk cohesion energy of transition metals as a function of the d band filling, within a rectangular model of the density of states (DOS) [17]. It is also the essence of a very successful model of surface reactivity [18]. The so-called second moment approximation (SMA), in which the DOS is represented by its first and second moments only [16], and the local neutrality condition have allowed

to decipher many surface properties, such as the narrowing of surface bands and the resulting photoemission core level shifts [19]. The SMA has also been widely used to represent the attractive many-body potential between metallic atoms due to band formation [20].

A similar tight binding method, equivalent of the NDO methods (NDO = Neglect of Differential Overlap) of chemistry [21], provides the generic features of the electronic structure of insulating oxides. However, in contrast to metals, it requires taking into account the charges Q_i borne by the ions and the strong Madelung electrostatic potentials V_i which result. Both are linked by the Poisson's equation. They modify the effective atomic orbital energies ϵ_i, approximately as [1]:

$$\epsilon_i = \epsilon_i^0 - U_i Q_i - V_i \tag{2}$$

Equation (2) tells that atomic levels ϵ_i^0 of the isolated neutral atoms i are shifted by intra-atomic electron–electron repulsion U_i when the atoms are charged and by the electrostatic potential V_i exerted by neighboring atoms. The two contributions are usually in competition — for example $U_i Q_i < 0$ and $V_i > 0$ on anions, and the opposite for cations — and their balance depends on the value of the optical dielectric constant which controls the screening properties.

Within this approach, the Mulliken electronegativity χ of an atom in the solid takes a very simple form. As characterizing the capability to donate or receive electrons, it is defined as the opposite of the first derivative of the total energy of the atom with respect to its electron number. It thus reads:

$$\chi_i = \chi_i^0 + U_i Q_i + V_i \tag{3}$$

This expression shows that the electronegativity χ_i of an *atom in a solid* is different from that of the isolated neutral atom χ_i^0 and strongly depends on the local atomic arrangements. It may be used as a guideline to predict the *variations* of ionization potentials and electron affinities as a function of the atom environment, as well as their basicity and acidity [1].

Since the ϵ_i depend on the charges and the charges on the ϵ_i, a self-consistent procedure is required to solve the electronic structure. Application of this method confirms that most oxides are only partially ionic, with some electron sharing between anions and cations. Although they are not measurable quantities, charges play a central role in the description of insulating oxides. Various evaluation schemes have been proposed in the past, including the frequently used Mulliken [22] and Bader [23] analysis. Within the tight binding approach, starting from the purely ionic limit, in which oxygens and cations bear formal charges (Q_O^0 and Q_C^0, respectively), the electron sharing due to orbital overlap can be recast as a sum of bond contributions $\Delta_{O_iC_j}$, consistently with physical intuition [24,25]:

$$Q_{O_i} = Q_O^0 + \sum_{C_j} \Delta_{O_iC_j} \qquad Q_{C_j} = Q_C^0 - \sum_{O_i} \Delta_{O_iC_j} \tag{4}$$

The electron transfers per bond $\Delta_{O_iC_j}$ are easily expressed as:

$$\Delta_{O_iC_j} = 1 - \frac{\epsilon_{C_j} - \epsilon_{O_i}}{\sqrt{(\epsilon_{C_j} - \epsilon_{O_j})^2 + 4\beta_{ij}^2}} \approx \frac{2\beta_{ij}^2}{(\epsilon_{C_j} - \epsilon_{O_i})^2} \tag{5}$$

They vanish in the ionic limit (either $\beta_{ij} = 0$ or $\epsilon_{C_j} - \epsilon_{O_i} \to \infty$) and vary monotonically with the ratio $\beta_{ij}/(\epsilon_{C_j} - \epsilon_{O_i})$, as evident in the perturbative expression in the right hand side of Equation (5). Their magnitude thus characterizes the covalent strength of the bonding and is directly related to the local electronic properties of the two bound atoms. Therefore, their analysis provides a simple way to characterize the variable ionic and covalent contributions to the bonds in various environments.

The environment effect lies in the variations of the ϵ_i with the Madelung potential. For example, at under-coordinated sites where V_i is reduced, the oxygen and cation effective levels are closer to each other than in the bulk (Fig. 1), rendering bonds more covalent. We have evidenced this effect in small neutral or charged stoichiometric TiO_2 clusters, TiO_2 bulk rutile and (110) surface [24]. We have performed a decomposition of the inhomogeneous electron density issued from DFT simulations, following Bader's prescription [23] and obtained oxygen and cation charges Q_{O_i} and Q_{C_j} by integration inside their atomic basins. The inequivalent $\Delta_{O_iC_j}$ were subsequently determined by inversion of Equation (4). Fig. 1 displays the values of the $\Delta_{O_iC_j}$ for each bond in these systems, as a function of the difference δV_{Mad} of the Madelung potentials V_O and V_{Ti} acting on the Ti and O atoms and as a function of the Ti–O bond lengths d. The good correlation with δV_{Mad} supports the simplified expression Equation (5), and the correlation with the bond length — a measurable quantity — assesses the relevance of the $\Delta_{O_iC_j}$ to characterize the degree of covalency of the bonds. It is striking to observe that, in a relatively covalent oxide like TiO_2, the covalent character varies so strongly with the local environment of the atoms.

In insulating charge-transfer compounds, the tight-binding method provides an approximate expression for the LDOS on an alternating lattice [26,1]. At the level of the second moment approximation, one obtains the energy separation ΔE_{VC} between the centers of gravity of the valence (VB) and conduction (CB) bands:

$$\Delta E_{VC} = \sqrt{(\epsilon_C - \epsilon_O)^2 + 4Z\beta^2} \tag{6}$$

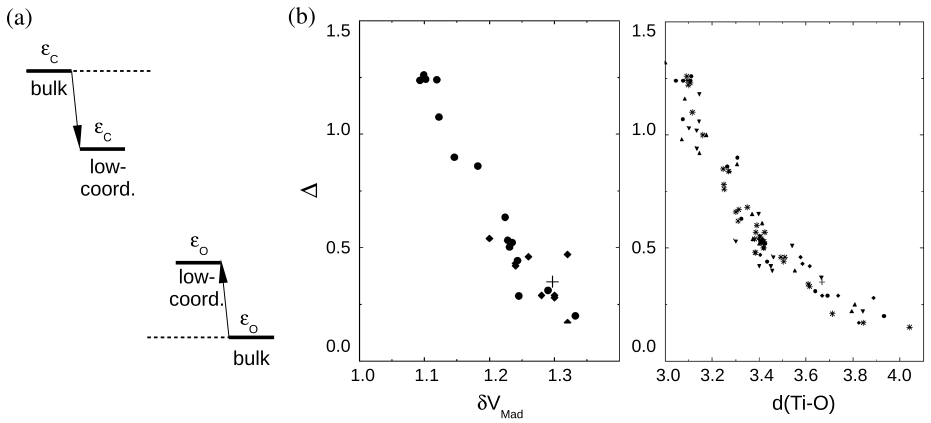

Fig. 1. (a): Shifts of the cation and oxygen effective atomic orbital energies ϵ_C and ϵ_O between a bulk and a low-coordinated environment, due to the reduction of the Madelung potential. (b): Electron transfer Δ per Ti–O bond as a function of the difference δV_{Mad} of the Madelung potentials acting on the Ti and O atoms (in Hartree per electron), and as a function of the Ti–O bond length d(Ti–O) (in atomic units). Results for neutral stoichiometric clusters, charged clusters, bulk rutile TiO_2 and TiO_2(110) surface are represented by filled circles, stars, plus signs and diamonds, respectively (from Reference [24]).

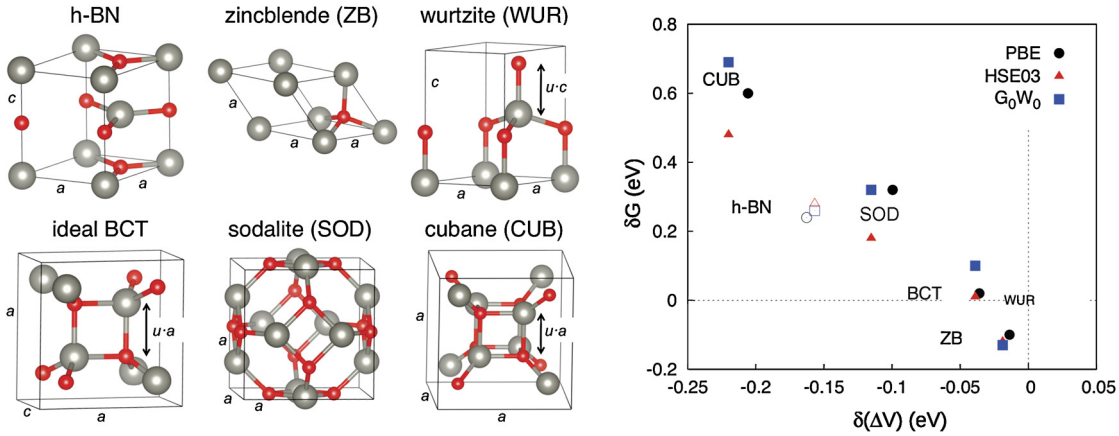

Fig. 2. Left panels: Primitive cells of six ZnO polymorphs. Small red balls are O atoms, big gray ones are Zn. Right panel: Variations of the gap widths δG versus the variation of electrostatic potential difference $\delta(\Delta V)$, each with respect to its value in the wurtzite structure. The negative slope points towards band width effects rather than electrostatic modifications of $\epsilon_C - \epsilon_O$. Black, red and blue symbols refer to different levels of approximation in the simulation (from Reference [28]).

ΔE_{VC} increases both with the separation of cation and oxygen levels $\epsilon_C - \epsilon_O$ and with the oxygen–cation hybridization, function of the resonance integrals β and the atom coordination number Z. The values of $\epsilon_C - \epsilon_O$ to be used are those relevant for the local environment of the atoms under consideration, taking into account their charge and the Madelung potential acting on them (Equation (2)). In most oxides, the Madelung term is dominant, which leads to an increase in ΔE_{VC} in more compact environments. The expression of ΔE_{VC} is reminiscent of Phillips' expression $E_g = \sqrt{E_h^2 + E_c^2}$ of the gap in semi-conductors [27], in which E_h and E_c were empirically defined as the heteropolar and covalent contributions, respectively. However, strictly speaking, this expression only applies to the energy separation between the centers of gravity of the VB and CB, not to the gap width. For the latter, the nature and symmetry of the orbitals involved at the relevant points of the Brillouin Zone are crucial, leading in some cases to a cancellation of the covalent contribution. Moreover, in E_g as well as in ΔE_{VC}, only anion–cation hybridization is taken into account. The oxygen–oxygen as well as the cation–cation hybridizations, although less efficient than the oxygen–cation one, may modify the LDOS. In particular, they participate in an increase of the band widths at the top of VB and bottom of CB in stoichiometric charge transfer insulating oxides where the HOMO level is usually strongly localized on the oxygens, and the LUMO level has a prevalent cation character. Such effects lead to a reduction in the band gap in more compact environments, as exemplified in Fig. 2 from a recent study of ZnO bulk polymorphs [28].

Besides providing interpretative tools to understand electronic structure features of complex systems, the self-consistent tight-binding method combined with an order-N algorithm represents an efficient basis for the study of large systems [29]. Indeed, the most time consuming part of the electronic structure calculation is the diagonalization of the Hamiltonian matrix, which roughly scales as the cube of the number N of valence electrons in the system, and which has to be repeatedly performed until self consistency is achieved. In order to transform the N^3 scaling into a linear scaling, a "divide-and-

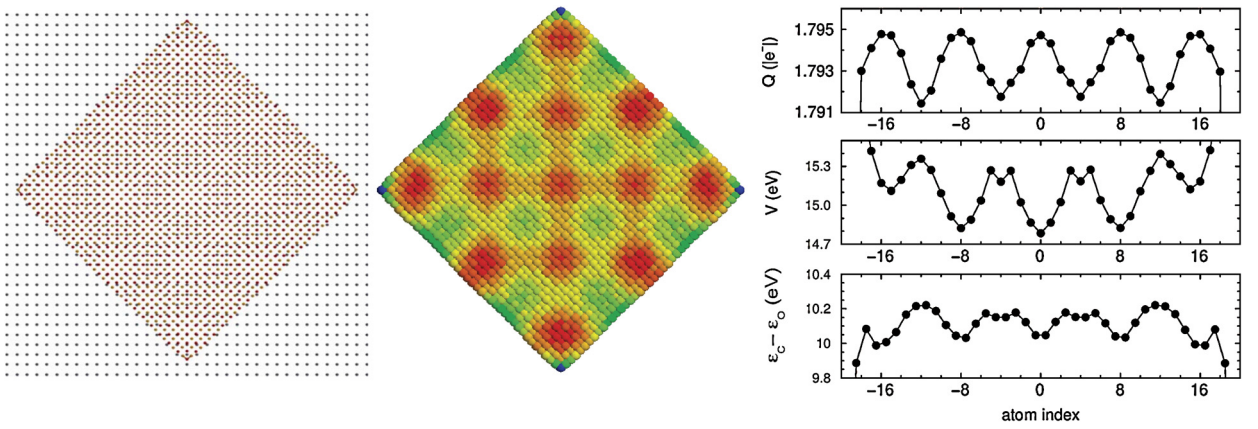

Fig. 3. From left to right: structure of an MgO(100) island deposited on a metal substrate, with gray, red and green dots representing substrate, oxygen and magnesium atoms, respectively. Color representation of the mean Mg–O distance $< d_{\mathrm{Mg-O}} >$ around each atom (larger to smaller from red to green). Local electronic property profiles across the island diagonal: Top panel: absolute values of Bader charges Q; Middle panel: electrostatic potential V on oxygen atoms; Lower panel: $\epsilon_C - \epsilon_O$ values on neighboring atoms.

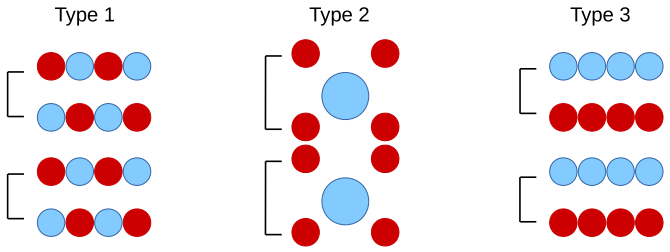

Fig. 4. Classification of compound surfaces (profile views) according to Tasker [30]. At type-1 surfaces, the layers are neutral and the repeat unit bears no dipole moment. In more complex crystallographic structures, the layers are non-neutral, but when the repeat unit bears no dipole moment, as schematized in type-2 surfaces, the surfaces are stable. At type-3 surfaces, both the layer charge and the dipole moment borne by the repeat unit are non-zero. These "polar" surfaces are unstable.

conquer" strategy may be implemented. The system is divided into overlapping clusters centered on each atom, containing n valence electrons and in which up to m electron hoppings may take place (effective m neighboring shells). The Hamiltonian matrix is built and diagonalized for each of these clusters and the LDOS on the central atoms only is retained. It may be shown that it is exact up to its m first moments. The sum of these LDOS gives the total density of states, from which the Fermi level position is deduced, as well as the density matrix which is then used for the next self-consistency step. Thanks to the replacement of a large $N \times N$ matrix diagonalization by a sequence of diagonalizations of smaller $(n \times n)$ matrices, the computational cost grows as $N \times n^3$ and linear scaling as a function of N is achieved. It is a method of choice for insulating systems in which the relative localization of the one-electron wave functions allows to chose small cluster sizes.

An application to MgO islands on (100) surfaces of fcc metals [29] is shown in Fig. 3, as an example of weak to moderate island-support interaction. The lattice mismatch between the oxide layer and the metallic substrate induces a nano-structured pattern made of a network of interfacial dislocations, which release the misfit strain. The dislocation regions are characterized by local structural (bond length variations, modification of the elevation of the atoms) and electronic (charges, work function) properties different from those in the regions of good lattice matching. This creates a peculiar energetic landscape for adsorbates, which favors self-assembly processes.

3. Specificities of oxide surfaces and ultra-thin films

Compared to metals or tetrahedral semiconductors, oxides present an impressive variety of crystallographic structures which are reflected in the atom organization at their surfaces. Except for the simplest structures, usually, several terminations may be produced along a given surface orientation. Moreover, by tuning the experimental conditions, such as temperature or partial gas pressures (oxygen and water), surfaces of different compositions may be stabilized.

Among this diversity, a classification exists, which is based on electrostatic arguments [30]. Three types of surfaces are differentiated, according to whether the structural repeat unit starting from vacuum bears a charge and/or a dipole moment (Fig. 4). While type-1 and type-2 surfaces (non-polar surfaces) are usually the most stable, with no dipole moment in their repeat units, type-3 surfaces (polar surfaces) experience a strong electrostatic instability.

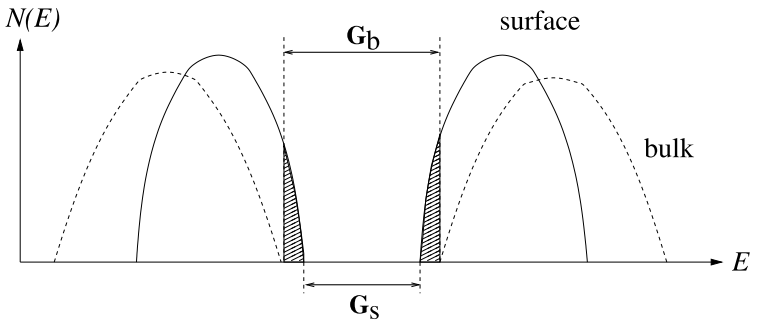

Fig. 5. Schematic representation of bulk (dashed lines) and surface (plain lines) DOS in insulating oxides. The surface VB and CB bands are more narrow than bulk bands and closer to each other, thus diminishing the gap width G_s with respect to the bulk value G_b. The gray shading thus denotes surface states.

3.1. Non-polar surfaces and ultra-thin films

Atoms at stoichiometric non-polar surfaces are characterized by a coordination lower than in the bulk. According to the arguments given above, their effective atomic levels ϵ_{C_j} and ϵ_{O_i} come closer to each other, due to the decrease of the Madelung potential. The covalent character of the bonds thus increases and this is amplified by relaxation effects that quite systematically induce bond contraction (the values of β_{ij} increase). The bands are thus distorted and shifted, but, in many cases, the Madelung effect is dominant. As shown schematically in Fig. 5, surface states appear in the gap, close to the band edges. A narrowing of the gap thus takes place, which is confirmed by experimental results or more advanced theoretical simulations in compounds such as MgO [31,32], CaO [33], NiO [34] or Al_2O_3 [35]. This trend is opposite to what is found in tetrahedral semiconductors nanostructures, where confinement effects combined with large covalent interactions lead to a gap widening.

During surface preparation, if annealing is performed under ultra-high vacuum (UHV), oxygen loss is likely to occur in the outermost layers. Depending upon the annealing temperature and duration, surfaces with under-stoichiometry in oxygen may be produced. Before this fact was fully recognized, it was claimed that oxide surfaces displayed many surface states in their gap. However, the states that had been observed were not intrinsic surface states, but rather oxygen vacancy states. Indeed, when a neutral oxygen desorbs, it leaves behind two electrons. Depending upon the relative value of the gap width and of the Madelung potential acting at the vacancy site, either these electrons are trapped at the vacancy site (highly ionic oxide) or they localize on the neighboring cations (small gap oxides like TiO_2), thus changing the cation's oxidation state [36]. When large vacancy densities are produced, the surface may even become metallic. This is likely the reason for the recent photoemission observation of a 2D electron gas at the surface of $SrTiO_3$ [37].

Many reconstructions have been observed at oxide non-polar surfaces. However, at variance with metals or semiconductors, they are not intrinsic but rather due to non-stoichiometry and are driven by vacancy ordering under specific preparation conditions. One of the richest diagram is displayed by the under-stoichiometric α-alumina (0001) surface. After annealing at increasing temperatures, a succession of reconstruction patterns has been observed: (1×1), $(\sqrt{3} \times \sqrt{3})R30°$, $(2\sqrt{3} \times 2\sqrt{3})R30°$, $(3\sqrt{3} \times 3\sqrt{3})R30°$ and $(\sqrt{31} \times \sqrt{31})R \pm 9°$ [38]. Each of them is associated with a different oxygen content in the outermost layers, the density of vacancy increasing with the annealing temperature. The most oxygen-deficient $(\sqrt{31} \times \sqrt{31})R \pm 9°$ configuration consists of hexagonal zones of two, nearly perfect, close-packed Al(111) planes separated by a defect of hexagonal periodicity [39]. Non-stoichiometric reconstructions have also been observed on TiO_2(100) [40] and many other non-polar surfaces.

Beyond semi-infinite surfaces, in the past decade, ultra-thin oxide films have become a very active field of research. Aside from their interest in solving the charging problem which prevents spectroscopic measurements to be performed on semi-infinite surfaces, they also represent model catalytic systems with very flexible structural and compositional characteristics. Playing with metal atom deposition rate, oxygen partial pressure and temperature allows stabilizing a rich variety of nearly 2D oxide phases, with chemical compositions unknown in the bulk. For example, the phase diagram of vanadium oxide on a Rh(111) substrate, in the sub-monolayer regime, displays a succession of phases at decreasing oxygen chemical potential: $(\sqrt{7} \times \sqrt{7})$ V_6O_{12}, (5×5) $V_{11}O_{28}$, $(5 \times 3\sqrt{3})$ $V_{13}O_{21}$, (9×9) $V_{36}O_{54}$ and "wagon-wheel" $V_{37}O_{17}$, associated with a decrease in the vanadium oxidation state and a progressive loss of vanadyl groups [41,42]. Similarly, at low coverage on Pd(100), MnO_x films display a complex surface phase diagram as a function of the oxygen chemical potential, with nine different phases associated with different oxidation states of Mn (Fig. 6) [43].

In the ultra-thin regime, when films are supported on a metal substrate, a number of new effects takes place, which have implications on the film structure and the metal work function. First, a charge transfer between film and support takes place, whose sign depends on the relative position of the metal Fermi level (its electronegativity) and the oxide point of zero charge. For example, for a single MgO(111) monolayer [44], deposition on a simple metal (Mg, Al) results in an electron transfer from the substrate to the film, while on transition metal substrates (Ag, Mo, Pt) electrons are transferred in the opposite direction. While perfectly flat when unsupported, oxide monolayers may get rumpled upon deposition

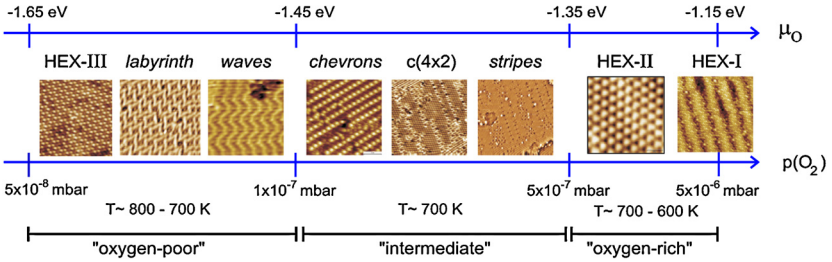

Fig. 6. Complex phase diagram of MnO_x/Pd(100) films as a function of the oxygen chemical potential μ_O or partial pressure $p(O_2)$ (from reference [43]).

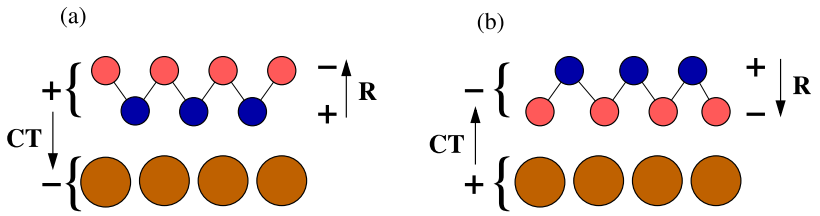

Fig. 7. Schematic representation of the charge transfer (CT) and rumpling (R) dipole moments (shown by arrows), for the two cases of negative (a) and positive (b) metal charging. In the first case, oxygen atoms of the oxide film are repelled by the negative charge of the metal and pushed outwards. In the second case, they are attracted by the substrate. Cations, oxygens and metal atoms are represented by blue, red and brown circles, respectively.

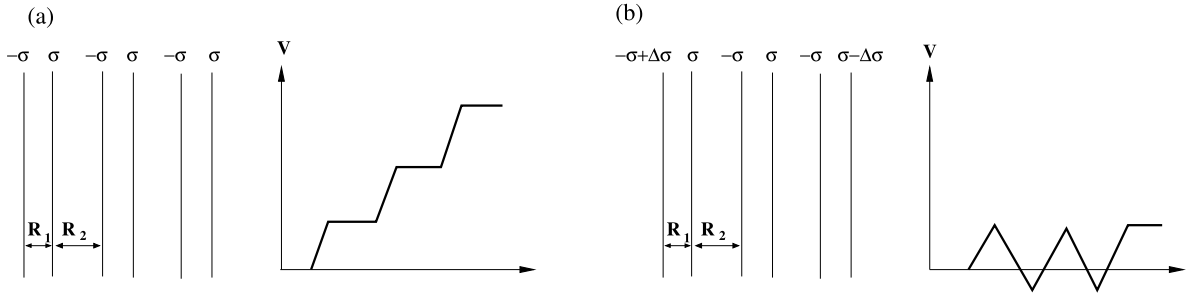

Fig. 8. (a): Capacitor model of a polar surface with alternating layers of charge density $\pm\sigma$ and spatial variation of the electrostatic potential V. (b): same but compensating charges $\Delta\sigma = \sigma R_1/(R_1 + R_2)$ are added on the outer layers, suppressing the monotonic variation of the electrostatic potential.

as a result of electrostatic interactions with the charge of the support (Fig. 7). The sign and strength of this structural polarization correlate with the interfacial charge transfer, in such a way that the associated dipoles have opposite signs and thus partially compensate each other [44]. Thus, as a whole, the modification of the metallic substrate work function includes three contributions: one due to the interfacial charge transfer, one due to the oxide film rumpling, and a third one due to the compression of the metal electrons at the interface with the oxide film. The relative strength of these three contributions is sensitive to the local interface structure, in particular the interfacial strain and the resulting misfit dislocations [45]. It is also critical for the charging of adsorbed species, with implications on the growth, chemical, optical, and magnetic properties of adsorbed metal particles and their self-organization [46].

Finally, the possible exchange of electrons between the oxide film and the support may in some cases help stabilizing very unexpected oxide stoichiometries. For example, exposition of an FeO(111) monolayer supported on a Pt(111) single crystal to an oxygen partial pressure in the millibar range results in a charged OFeO trilayer, with the iron atoms in a 3+ oxidation state and a missing electron per formula unit coming from the Pt substrate. The FeO_2 trilayer may then serve as an oxygen reservoir for the oxidation of CO, which explains the greatly enhanced reactivity of this system compared to the bare underlying substrate, under the same conditions [47].

3.2. Polar surfaces and ultra-thin films

The specificity of polar surfaces (type-3 surfaces in Tasker's classification [30]) comes from the combined effect of orientation and termination, responsible for the existence of a macroscopic polarization along the surface normal. For a long time, it has been believed that these surfaces do not exist because an infinite surface energy results from this polarization. Indeed, as shown by a simple capacitor model of alternating layers with charges densities $\pm\sigma$ (Fig. 8), the electrostatic potential varies monotonically across the system, inducing surface instability. However, similarly to the case of ferroelectric materials, compensating charge densities on the outer surfaces, equal to:

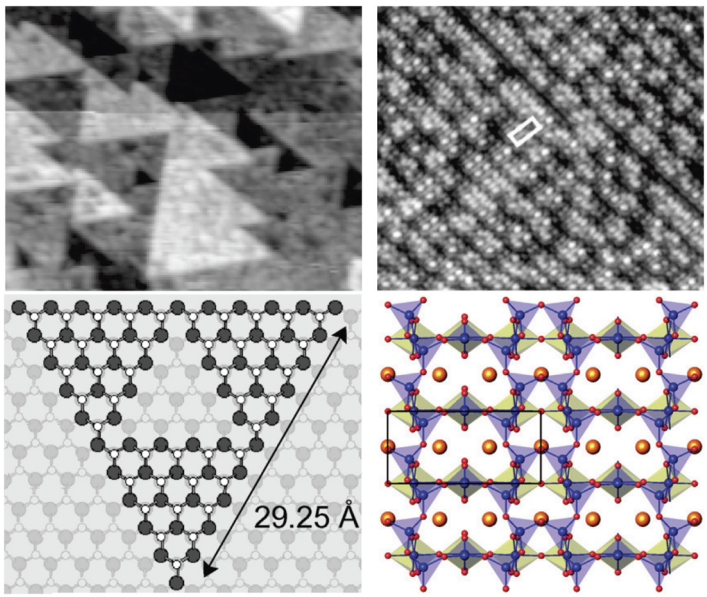

Fig. 9. Left panels: STM image of the Zn-terminated ZnO(0001) surface and atomistic model of magic triangles (from reference [50]). Right panels: STM images [52] and model [51] of the reconstructed $SrTiO_3(110)$ (3×1) surface. Surface TiO_4 tetrahedra are shown in blue, bulk TiO_6 octahedra in yellow, oxygen anions in red and strontium cations in orange.

$$\Delta\sigma = \sigma \frac{R_1}{(R_1 + R_2)} \tag{7}$$

may stabilize polar surfaces by creating the required depolarization field. Indeed many polar oxide surfaces have been prepared and studied in the past, such as MgO(111), ZnO(0001), $SrTiO_3(110)$ or (111), $Fe_3O_4(100)$ and this field remains very active [48,49].

The necessary charge compensation may be achieved in many ways: by a deep modification of the surface electronic structure — total or partial filling of surface states, sometimes leading to surface metallization — or by strong changes in the surface stoichiometry — spontaneous desorption of ions, faceting, large cell reconstructions due to the ordering of charged vacancies —, adsorption of foreign ionized species, etc. These processes have led to original surface configurations, in which the local environment of the surface atoms is very different from the bulk or from non-polar terminations. Fig. 9 shows examples of polar surface configurations, involving missing ions in the outer layers, with just the right density to fulfill the electrostatic criterion, Equation (7). In the first case [50], the ZnO(0001) surface atoms form triangular nanoislands or pits with no long-range order, while on $SrTiO_3(110)$ numerous ordered reconstructions have been observed [51]. This quick overview shows that, contrary to initial expectations, polar surfaces are of prominent interest, from many points of view.

In the last decade, this fascinating field has evolved towards polar nanostructures, largely stimulated by the growing demand for novel materials for applications in microelectronics and heterogeneous catalysis. This is particularly true for ultra-thin films, made of only a few atomic layers stacked along a polar direction, which have been shown to display a variety of new characteristics. There have also been advances in the controlled fabrication of small polar oxide objects, such as nanoribbons, nanoislands, and nanoclusters, in view of novel applications in optoelectronics, sensors, transducers, and biomedical sciences [53].

Polar nano-objects raise a number of very new questions related to finite-size effects and the role of dimensionality in driving the polar instability. As compared to semi-infinite surfaces, additional mechanisms of polarity compensation exist at the nanoscale. On the one hand, in sufficiently thin polar films, since there is no actual divergence of the electrostatic potential, polarization may be sustained [54]. On the other hand, it has been shown that, at very small thickness, wurtzite ZnO(0001) [55] and rocksalt MgO(111) [56] polar films avoid polarity by changing their structure to (0001) hexagonal BN. In these oxides, but also in AlN, BeO, GaN, SiC, and ZnS films, at the nanoscale, the surface and bulk energy contributions are in competition: inner atoms in the film are better stabilized in the bulk ground-state structure, while the (0001) hexagonal BN structure is more favorable to surface atoms because it is non-polar. In ultra-thin films (a few monolayers), the surface terms are able to overcome the bulk ones up to a given critical thickness. More recently, we showed [57,58] that the equivalent of surface polarity in thin films is edge polarity in polar nano-ribbons, and we found that very narrow zigzag ribbons cut out of $MoSe_2$ trilayers change stacking from 1H to 1T to avoid polarity, in a way quite similar to what happens in ZnO(0001) or MgO(111) thin films (Fig. 10).

Aside from these complete changes of structures, strong lattice relaxations or inhomogeneous charge redistributions, among others, may also occur. Because most nano-objects are grown on (metallic or insulating) substrates, there is an interplay between polarity and substrate effects: interfacial charge transfer, adhesion, and lattice mismatch, particularly

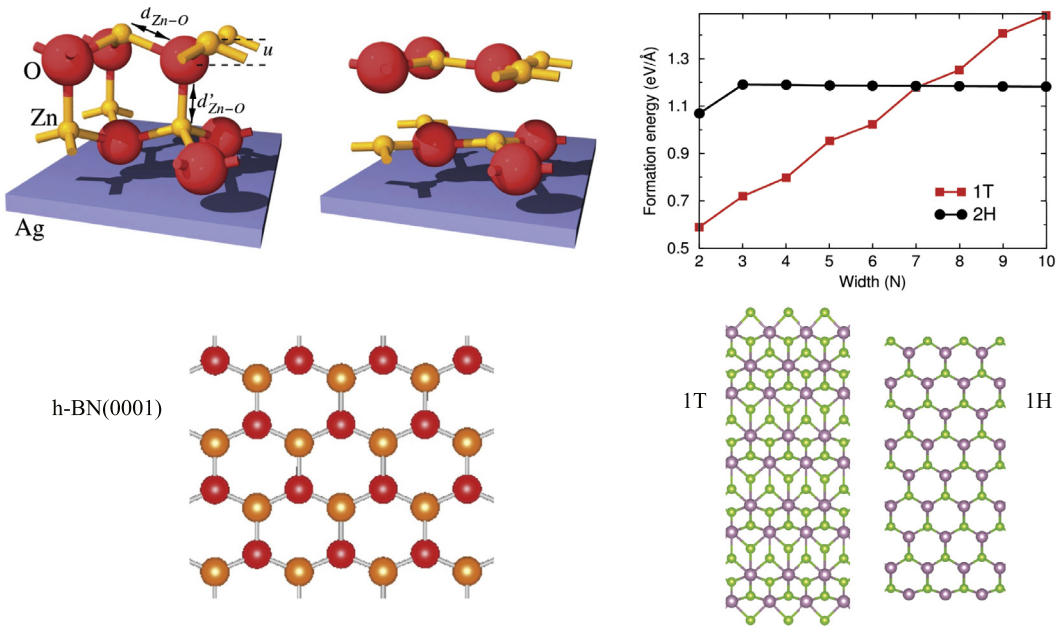

Fig. 10. Left panels: transformation of a ZnO(0001) bilayer from wurtzite to h-BN structure and top view of a h-BN(0001) layer [55]. Right panels: phase transition of a MoS_2 polar zig-zag nano-ribbon as a function of width and top view of 1H and 1T ribbon structures [58]. Mo and S atoms are represented by large gray and small yellow balls, respectively.

important for the stability of monolayer films or 2D polar objects. Finally, the understanding of the 2D or 1D electron gases present at some polar interfaces or at polar island edges is related to the very hot physics of confinement effects in new layered materials.

4. Prospects

During 25 years of intense research, the field of oxide surfaces has enormously developed. At semi-infinite surfaces, the fine description and understanding of reconstructions, whether at non-polar or polar terminations, remains a challenge due to the variety of configurations that may be produced under different preparation conditions. The same is true in ultra-thin films, in which 2D oxides of structure and stoichiometry unknown in the bulk may be produced. Their application to electronic devices or catalysis are not yet fully explored.

The control of structure, shape, composition and size distribution of nano-oxides — nano-clusters, stripes, nano-islands — is not a simple matter. It involves a delicate interplay between thermodynamic and kinetic parameters in the preparation protocol. As for their characterization, atomic resolution can be achieved in a number of cases, but the question of atom recognition, for the determination of their local stoichiometry, remains largely unsolved. Yet, many groups devote efforts in their preparation, in view of the possibility of engineering some of their properties — reactivity, magnetic, optical — via shape or size control.

Besides conditions of gaseous or UHV environment, nano-oxides may also be prepared by soft chemistry methods or may be formed in the natural environment as a result of rock weathering. The interaction with an aqueous medium modifies the surface charges and the ordering of surface energies, and thus the particles' shapes and sizes. Present efforts are mainly focused on obtaining very anisotropic particles for optical applications, or high-energy surfaces for reactivity purposes.

Finally, the long-lasting interest in low-dimensional electron gases produced by confinement effects nowadays turns towards oxide surfaces, interfaces and nano-objects. For example, a 2D electron gas has been evidenced at the perovskite $LaAlO_3/SrTiO_3(001)$ interface. There is not yet a definite answer to whether it is due to polarity ($LaAlO_3(001)$ is a polar orientation) or to another origin, such as non-stoichiometry, but the topic remains very hot, with extensions towards polar/polar interfaces, either between thin films or nano-ribbons.

All these quickly sketched questions will undoubtedly prompt or continue to prompt a high activity in the scientific community in the coming years, with a richness coming from many inter-disciplinary links and view points.

References

[1] C. Noguera, Physics and Chemistry at Oxide Surfaces, Cambridge University Press, Cambridge, 1996, 2005.
[2] M. Born, K. Huang, Dynamic Theory of Crystal Lattices, Oxford University Press, London, 1954.
[3] S.M. Woodley, P.D. Battle, J.D. Gale, C.R.A. Catlow, Phys. Chem. Chem. Phys. 1 (1999) 253.
[4] W.C. Mackrodt, R.J. Davey, S.N. Black, R. Docherty, J. Cryst. Growth 80 (1987) 441.

[5] P. Geysermans, C. Noguera, J. Mater. Chem. 19 (2009) 7807.
[6] J.A. Purton, N.L. Allan, M.Yu. Lavrentiev, I.T. Todorov, C.L. Freeman, Chem. Geol. 225 (2006) 176.
[7] F.H. Streitz, J.W. Mintmire, Phys. Rev. B 50 (1994) 11996.
[8] D.M. York, W. Yang, J. Chem. Phys. 104 (1996) 159.
[9] A. Hallil, R. Tétot, F. Berthier, I. Braems, J. Creuze, Phys. Rev. B 73 (2006) 165406.
[10] T. Campbell, R.K. Kalia, A. Nakano, P. Vashishta, S. Ogata, S. Rodgers, Phys. Rev. Lett. 82 (1999) 4866.
[11] J. Zaanen, G.A. Sawatzky, J. Solid State Chem. 88 (1990) 8.
[12] W. Kohn, C.D. Sherrill, J. Chem. Phys. 140 (2014) 18A201.
[13] Special topics, J. Chem. Phys. 140 (18) (2014).
[14] A.D. Becke, J. Chem. Phys. 98 (1993) 1372;
J.P. Perdew, M. Ernzerhof, K. Burke, J. Chem. Phys. 105 (1996) 9982.
[15] T. Tsuneda, K. Hirao, J. Chem. Phys. 140 (2014) 18A513, and references therein.
[16] F. Cyrot-Lackmann, F. Ducastelle, Phys. Rev. B 4 (1971) 2406–2412.
[17] J. Friedel, C.M. Sayers, J. Phys. (Paris) 38 (1977) 697.
[18] B. Hammer, J.K. Norskov, Adv. Catal. 45 (2000) 71.
[19] M.C. Desjonquères, D. Spanjaard, Y. Lassailly, C. Guyot, Solid State Commun. 34 (1980) 807.
[20] D. Pettifor, Bonding and Structure of Molecules and Solids, Oxford University Press, 1995.
[21] J.A. Pople, D.P. Santry, G.A. Segal, J. Chem. Phys. 43 (1965) S129.
[22] R.S. Mulliken, J. Chem. Phys. 23 (1955) 1833.
[23] R.F.W. Bader, Chem. Rev. 91 (1991) 983.
[24] T. Albaret, F. Finocchi, C. Noguera, Faraday Discuss. 114 (1999) 285.
[25] C. Noguera, A. Pojani, P. Casek, F. Finocchi, Surf. Sci. 507–510 (2002) 245.
[26] J.P. Julien, D. Mayou, F. Cyrot-Lackmann, J. Phys. (Paris) 50 (1989) 2683.
[27] J.C. Phillips, Rev. Mod. Phys. 42 (1970) 317.
[28] L. Sponza, J. Goniakowski, C. Noguera, Phys. Rev. B 91 (2015) 075126.
[29] C. Noguera, J. Godet, J. Goniakowski, Phys. Rev. B 81 (2010) 155409.
[30] P.W. Tasker, J. Phys. C, Solid State Phys. 12 (1979) 4977.
[31] F. Didier, J. Jupille, Surf. Sci. 307–309 (1994) 587.
[32] J. Goniakowski, C. Noguera, Surf. Sci. 323 (1995) 129.
[33] A.R. Protheroe, A. Steinbrunn, T.E. Gallon, Surf. Sci. 126 (1983) 534.
[34] S.L. Dudarev, A.I. Liechtenstein, M.R. Castell, G.A.D. Briggs, A.P. Sutton, Phys. Rev. B 56 (1997) 4900.
[35] M. Gautier-Soyer, F. Jollet, C. Noguera, Surf. Sci. 352–354 (1996) 755.
[36] F. Finocchi, J. Goniakowski, C. Noguera, Phys. Rev. B 59 (1999) 5178;
C.M. Yim, C.L. Pang, G. Thornton, Phys. Rev. Lett. 104 (2010) 036806.
[37] A.F. Santander-Syro, O. Copie, T. Kondo, F. Fortuna, S. Pailhes, R. Weht, X.G. Qiu, F. Bertran, A. Nicolaou, A. Taleb-Ibrahimi, P. Le Fèvre, G. Herranz, M. Bibes, N. Reyren, Y. Apertet, P. Lecoeur, A. Barthélémy, M.J. Rozenberg, Nature 469 (2011) 189.
[38] M. Gautier, J.P. Duraud, L. Van Pham, M.J. Guittet, Surf. Sci. 250 (1991) 71.
[39] M. Gautier, G. Renaud, L. Van Pham, B. Villette, M. Pollak, N. Thromat, F. Jollet, J.P. Duraud, J. Am. Ceram. Soc. 77 (1994) 323.
[40] M. Bowker, Curr. Opin. Solid State Mater. Sci. 10 (2006) 153.
[41] J. Schoiswohl, M. Sock, S. Eck, S. Surnev, M.G. Ramsey, F.P. Netzer, G. Kresse, Phys. Rev. B 69 (2004) 155403.
[42] J. Schoiswohl, S. Surnev, M. Sock, S. Eck, M.G. Ramsey, F.P. Netzer, G. Kresse, Phys. Rev. B 71 (2005) 165437.
[43] F. Li, G. Parteder, F. Allegretti, C. Franchini, R. Podloucky, S. Surnev, F.P. Netzer, J. Phys. Condens. Matter 21 (2009) 134008.
[44] J. Goniakowski, C. Noguera, Phys. Rev. B 79 (2009) 155433.
[45] S. Benedetti, F. Stavale, S. Valeri, C. Noguera, H.J. Freund, J. Goniakowski, N. Nilius, Adv. Funct. Mater. 23 (2013) 75.
[46] H.J. Freund, G. Pacchioni, Chem. Soc. Rev. 37 (2008) 2224.
[47] Y.-N. Sun, L. Giordano, J. Goniakowski, M. Lewandowski, Z.-H. Qin, C. Noguera, S. Shaikhutdinov, G. Pacchioni, H.-J. Freund, Angew. Chem., Int. Ed. 49 (2010) 4418.
[48] C. Noguera, J. Phys. Condens. Matter 12 (2000) R367.
[49] J. Goniakowski, F. Finocchi, C. Noguera, Rep. Prog. Phys. 71 (2008) 016501.
[50] O. Dulub, U. Diebold, G. Kresse, Phys. Rev. Lett. 90 (2003) 016102.
[51] J.A. Enterkin, A.K. Subramanian, B.C. Russell, M.R. Castell, K.R. Poeppelmeier, L.D. Marks, Nat. Mater. 9 (2010) 245.
[52] B.C. Russell, M.R. Castell, Phys. Rev. B 77 (2008) 245414.
[53] C. Noguera, J. Goniakowski, Chem. Rev. 113 (2013) 4073.
[54] J. Goniakowski, C. Noguera, L. Giordano, Phys. Rev. Lett. 98 (2007) 205701.
[55] C. Tusche, H.L. Meyerheim, J. Kirschner, Phys. Rev. Lett. 99 (2007) 026102.
[56] J. Goniakowski, C. Noguera, L. Giordano, Phys. Rev. Lett. 93 (2004) 215702.
[57] F. Güller, A.M. Llois, J. Goniakowski, C. Noguera, Phys. Rev. B 87 (2013) 205423.
[58] F. Güller, A.M. Llois, J. Goniakowski, C. Noguera, Phys. Rev. B 91 (2015) 075407.